

This is the accepted manuscript made available via CHORUS. The article has been published as:

## Efficient repumping of a Ca magneto-optical trap

Michael Mills, Prateek Puri, Yanmei Yu, Andrei Derevianko, Christian Schneider, and Eric R. Hudson

Phys. Rev. A **96**, 033402 — Published 5 September 2017

DOI: [10.1103/PhysRevA.96.033402](https://doi.org/10.1103/PhysRevA.96.033402)

# Improved magneto-optical trapping of Ca

Michael Mills,<sup>1</sup> Prateek Puri,<sup>1</sup> Yanmei Yu,<sup>2,3</sup> Andrei Derevianko,<sup>3</sup> Christian Schneider,<sup>1</sup> and Eric R. Hudson<sup>1</sup>

<sup>1</sup>*Department of Physics and Astronomy, University of California – Los Angeles, Los Angeles, California, 90095, USA*

<sup>2</sup>*Beijing National Laboratory for Condensed Matter Physics,*

*Institute of Physics, Chinese Academy of Sciences, Beijing 100190, China*

<sup>3</sup>*Department of Physics, University of Nevada, Reno, Nevada 89557, USA*

(Dated: August 3, 2017)

We investigate the limiting factors in the standard implementation of the Ca magneto-optical trap. We find that intercombination transitions from the  $4s5p\ ^1P_1$  state used to repump electronic population from the  $3d4s\ ^1D_2$  state severely reduce the trap lifetime. We explore seven alternative repumping schemes theoretically and investigate five of them experimentally. We find all five of these schemes yield a significant increase in trap lifetime and consequently improve the number of atoms and peak atom density by as much as  $\sim 20\times$  and  $\sim 6\times$ , respectively. One of these transitions, at 453 nm, is shown to approach the fundamental limit for a Ca magneto-optical trap with repumping only from the dark  $3d4s\ ^1D_2$  state, yielding a trap lifetime of  $\sim 5$  s.

## I. INTRODUCTION

The magneto-optical trap (MOT) [1] is an integral part of atomic and molecular physics, where it is the starting point for a variety of experiments including precision tests of fundamental physics [2], studies of quantum many-body physics [3], and production of ultracold molecules [4, 5]. At present, atomic MOTs have been constructed for atoms within Groups 1, 2, 6, 12, and 18, as well as the lanthanides. Extension to atoms in other Groups is often limited by the availability of appropriate laser technology for driving the necessary cooling transitions and complications due to the electronic structure of the atom. For example, if there are multiple electronic states below the upper electronic state of the primary laser cooling transition, then radiative decay into these lower levels can severely reduce, and even eliminate, the laser cooling force. For these reasons, the Group 1 atoms, with their lone optically active, unpaired electron, provide the simplest, and often best performing, MOTs.

Nonetheless, the same ‘complications’ that can limit the laser cooling process often host interesting and useful phenomena. A prime example of this is the presence of  $^3P$  states of Group 2(-like) atoms, which, while detrimental to the performance of a standard MOT, allow the construction of next-generation optical atomic clocks that can outperform the Cesium standard [6]. One such MOT of this type is the Ca MOT. Calcium MOTs have been utilized in atomic optical clock experiments using the 657 nm  $^3P_1 \leftarrow ^1S_0$  intercombination line [7–9] and have significant appeal due to their simplicity of construction as portable optical frequency standards [10]. However, despite this appeal, the details of the Ca electronic structure lead to relatively poor performance of Ca MOTs, including a short trap lifetime limited by optical pumping into dark states and a low achievable peak atomic density. This is one reason other Group 2(-like) atoms such as Sr, Yb, and Hg have become more popular choices for optical frequency standards [6, 11].

Given the potential of Ca as a portable frequency stan-

dard, as well as its utility in our own experiments as a sympathetic coolant for molecular ions [4], we have performed a detailed combined experimental and theoretical study of Ca MOT operation. Specifically, relativistic many-body calculations are performed for the first 75 energy levels of the Ca atom, providing reliable electronic structure and transition matrix elements for this multi-electron atom. The results of this calculation are incorporated into a rate equation model for the populations in the Ca atom, which is used to evaluate specific repumping schemes and identify seven promising transitions. In total, we experimentally investigate five alternative repumping schemes and find that all of them yield Ca MOTs with lifetimes and atom numbers improved by  $\sim 10\times$  over the traditional scheme described in Ref. [12]. The best of these schemes, which utilizes repumping to a highly configuration-mixed state with a 453 nm repumping laser, produces a Ca MOT with lifetime, number, and density improved over the standard MOT by  $\sim 25\times$ ,  $\sim 20\times$ , and  $\sim 6\times$ , respectively.

In the remainder of this paper, we first present the details of the relativistic many-body calculation of the Ca energy levels and the resulting rate equation model of the Ca populations. We then use this rate equation model to explain the poor performance of the traditional Ca MOT. From this work, we propose seven alternative MOT operation schemes and experimentally investigate five of them. We characterize the differences in these MOT operation schemes, reporting the achievable MOT lifetimes, density, and trapped atom numbers, as well as the necessary repumping laser frequencies. We conclude with discussion of the ideal repumping scheme for Ca MOT operation and possible extension to other Group 2(-like) atoms.

## II. RELATIVISTIC MANY-BODY CALCULATIONS OF ATOMIC STRUCTURE

The analysis of MOT performance requires estimates of electric-dipole transition rates between the 75 lowest-

States		$\Delta E$ , cm <sup>-1</sup>		$A_{if}$ , 10 <sup>8</sup> s <sup>-1</sup>		
Initial	Final	CI+MBPT	NIST	CI+MBPT	Exp.	Deviation (%)
4s4p <sup>1</sup> P <sub>1</sub>	4s <sup>2</sup> <sup>1</sup> S <sub>0</sub>	23491	23652.304	2.170	2.182(12) [13]	-0.5(5)
4p <sup>2</sup> <sup>1</sup> S <sub>0</sub>	4s4p <sup>1</sup> P <sub>1</sub>	18846	18133.972	0.778	0.754(21) [14]	3.2(2.9)
4p <sup>2</sup> <sup>1</sup> D <sub>2</sub>	4s4p <sup>1</sup> P <sub>1</sub>	17691	17067.543	0.576	0.683(11) [15]	-16(1)
3d4p <sup>1</sup> D <sub>2</sub>	3d4s <sup>1</sup> D <sub>2</sub>	13901	13985.779	0.341	0.358(9) [16]	-4.7(2.4)
4snp <sup>1</sup> P <sub>1</sub>	4s <sup>2</sup> <sup>1</sup> S <sub>0</sub>	44383	43933.477	0.325	0.284(39) [17]	14(16)
4s4f <sup>1</sup> F <sub>3</sub>	3d4s <sup>1</sup> D <sub>2</sub>	19943	20493.953	0.312	0.31(6) [18]	1(19)
4s7p <sup>1</sup> P <sub>1</sub>	4s <sup>2</sup> <sup>1</sup> S <sub>0</sub>	46975	45425.358	0.130	0.148(21) [18]	-12(12)
4s7s <sup>1</sup> S <sub>0</sub>	4s4p <sup>1</sup> P <sub>1</sub>	21724	20624.234	0.068	0.113(5) [14]	-40(3)
4s4d <sup>1</sup> D <sub>2</sub>	4s4p <sup>1</sup> P <sub>1</sub>	14169	13645.983	0.160	0.154(4) [14]	3.9(2.7)
4s6d <sup>1</sup> D <sub>2</sub>	4s4p <sup>1</sup> P <sub>1</sub>	22324	21337.526	0.057	0.080(3) [14]	-29(3)
4s5p <sup>1</sup> P <sub>1</sub>	3d4s <sup>1</sup> D <sub>2</sub>	14259	14881.981	0.130	0.147(3) [16]	-12(2)
4s6p <sup>1</sup> P <sub>1</sub>	4s <sup>2</sup> <sup>1</sup> S <sub>0</sub>	41788	41679.008	0.092	0.157(22) [17]	-41(8)
4s6s <sup>1</sup> S <sub>0</sub>	4s4p <sup>1</sup> P <sub>1</sub>	17451	17038.131	0.014	0.052(4) [14]	-73(2)
4s4p <sup>1</sup> P <sub>1</sub>	3d4s <sup>1</sup> D <sub>2</sub>	1041	1802.670	0.0000534	0.0000368(100) [18]	45(39)
4s4p <sup>3</sup> P <sub>1</sub>	4s <sup>2</sup> <sup>1</sup> S <sub>0</sub>	15180	15210.063	0.0000274	0.0000302(7) [19]	-9.3(2.2)
3d4p <sup>1</sup> F <sub>3</sub>	3d4s <sup>1</sup> D <sub>2</sub>	18651	18688.259	0.057	0.165(7) [16]	-65(1)

TABLE I. Comparison of CI+MBPT transition energies  $\Delta E$  (cm<sup>-1</sup>) and rates  $A_{if}$  (10<sup>8</sup> × s<sup>-1</sup>) with NIST-recommended transition energies and 16 out of the available 111 experimental transition rates along with their uncertainties.

energy levels of Ca, including both spin-allowed and spin-forbidden (intercombination) transitions. While the energy levels are well established, transition rates among the first 75 lowest-energy states (811 possible channels) are not known completely, although there are a number of theoretical and experimental determinations. The earlier theory work provides oscillator strengths for spin-allowed transitions for levels up to 4s10s, 4s9p, 4s6d, and 4s5f, respectively [20–23]. Most of these calculations are non-relativistic with a limited number of low-lying levels treated with *ab initio* relativistic methods. The data on transition probabilities for intercombination transitions and transitions involving the 4s6f states are scarce [24–26]. In literature, 111 experimental transition rates are available [13–19, 27–34]. The incompleteness of transition rate data motivated us to generate a full set of the 811 required transition rates. To this end we used methods of relativistic many-body theory. *Ab initio* relativistic calculations are necessary as the analysis requires inclusion of transition amplitudes that are non-relativistically forbidden.

Calcium is an atom with two valence electrons outside a tightly bound core. We employ a systematic formalism that combines advantages of both the configuration interaction (CI) method and many-body perturbation theory (MBPT), the CI+MBPT method [35]. The CI+MBPT method has been used extensively for evaluation of atomic properties (see, e.g., Ref. [36] for optical lattice clock applications and references therein). Relativistic effects are included exactly, as the formalism starts from the Dirac equation and employs relativistic bi-spinor wave functions throughout the entire calculation. In our treatment, the CI model space is limited to excitations of valence electrons. Contributions involving excitations of core electrons are treated within MBPT. In this approach, we first solve for the valence

electron orbitals and energies in the field of the core electrons. The one-electron effective potential includes both the frozen-core Dirac-Hartree-Fock (DHF  $V^{N-2}$ ) and self-energy (core-polarization) potentials. The self-energy correction is computed using second-order MBPT diagrams involving virtual core excitations. At the next step, the computed one-electron valence orbitals are used to diagonalize the atomic Hamiltonian in the model space of two valence electrons within the CI method. The CI Hamiltonian includes the residual (beyond DHF) Coulomb interaction between the valence electrons and their core-polarization-mediated interaction. The latter was computed in the second-order MBPT. This step yields two-electron wave-functions and energies. Finally, with the obtained wave-functions we calculated the required electric-dipole matrix elements. In calculations of transition rates we used experimental energy intervals and the computed CI+MBPT matrix elements.

We used two independent CI+MBPT implementations: (i) by the Reno group (see the discussion of the earlier version in Ref. [37]) and (ii) a recently published package [38]. The practical goal of the calculations was not to reach the highest possible accuracy, but rather to generate the large amount of data needed for the transition array involving the 75 lowest-energy levels. An additional computational challenge was the inclusion of high angular momenta states, e.g., the 4s5g <sup>3</sup>G state. The Reno code was run on a large basis set but without including core-polarization-mediated interaction in the CI Hamiltonian due to considerable computational costs. The production runs with the package of Ref. [38] employed a smaller basis set (due to code limitations) but treated the correlation problem more fully. Our final values combine the outputs of the two codes. The bulk of the results comes from the package of Ref. [38]. These results are augmented with the rate data involving 4s8s

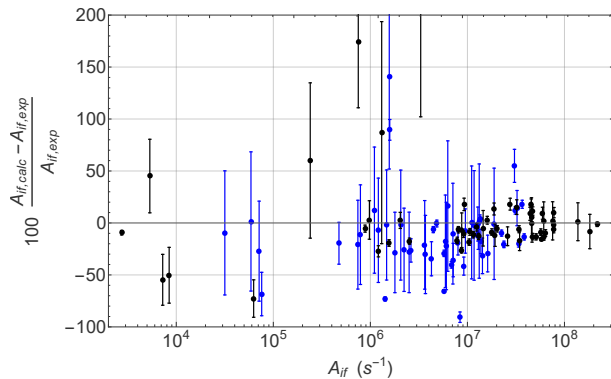


FIG. 1. Comparison of the calculated CI+MBPT transition rates with 111 available experimental data. Transitions involving a state with orbital angular momentum  $l \geq 3$  or principal quantum number  $n \geq 6$  are shown in blue. All other transitions are shown in black. Error bars correspond to the experimental error.

states from the Reno code due to the limited number of roots in the package of Ref. [38].

We assessed the quality of the calculations by comparing the CI+MBPT energies with the NIST recommended values [30] and CI+MBPT transition rates with 111 available experimental values (see subset in Table I)[13–19, 27–34]. The CI+MBPT energy intervals for tabulated transitions agree with NIST values to better than  $1000 \text{ cm}^{-1}$ . To quantify the error of the CI+MBPT transition rates, we calculate the relative deviation from the experimental values,  $E_{if} = 100 \frac{A_{if,calc} - A_{if,exp}}{A_{if,exp}}$ , with standard errors corresponding to the experimental errors (see Fig. 1). The weighted root mean square of  $E_{if}$  yields an estimate of the error of the CI+MBPT transition rates. We determine this error for two subsets of transitions: The first includes all transitions involving a state with orbital angular momentum  $l \geq 3$  or principal quantum number  $n \geq 6$ , where both faithful numerical representation and inclusion of correlations are important, and yields an average error of 48%. The second subset includes all other transitions and has an average error of 13%. This difference in error is reflective of the computational difficulty of obtaining transition rates for these subsets of transitions. For some transitions, the deviation of our theoretical transition rates from experiment is large; to remedy this, we replace our calculated transition rates with experimental values when the deviation is greater than twice the experimental error or the experimental error is less than our expected error. In the supplementary material, we provide the complete data set that includes all 811 calculated transitions, as well as a data set augmented by experimental values.

### III. RATE EQUATION MODEL OF Ca ELECTRONIC STATE POPULATIONS

Using the 811 calculated CI+MBPT transition rates augmented by experimental transition rates as previously described, we create a rate model including the first 75 excited states of calcium. As an example, the differential equation for state  $i$  with a monochromatic laser driving from state  $i$  to state  $k$  is given by

$$\begin{aligned} \frac{d}{dt} N_i = & \sum_{j>i} A_{ji} N_j - \sum_{j<i} A_{ij} N_i - \frac{N_i}{\tau_{Loss}} \\ & + A_{ki} \frac{\pi^2 c^3}{\hbar \omega_{ik}^3} \frac{I_l}{2\pi c} \frac{\Gamma_k}{(\omega_{ik} - \omega_l)^2 + \frac{\Gamma_k^2}{4}} \left( N_k - \frac{2j_k + 1}{2j_i + 1} N_i \right) \end{aligned} \quad (1)$$

where  $N_i$  is the number of atoms in state  $i$ ,  $A_{ij}$  is the decay rate of state  $i$  to  $j$ ,  $\tau_{Loss}$  is the time in which an uncooled atom drifts outside of the MOT region (for our parameters, this value is 1.7 ms for the  $4s4p \ ^3P_0$  and  $^3P_2$  states and  $\infty$  otherwise),  $c$  is the speed of light in a vacuum,  $\hbar$  is the reduced Planck constant,  $\omega_{ik}$  is the angular transition frequency between state  $i$  and  $k$ ,  $\omega_l$  ( $I_l$ ) is the angular frequency (intensity) of the applied laser,  $\Gamma_k$  is the natural linewidth of state  $k$ , and  $j_i$  is the total angular momentum quantum number of state  $i$  [39].

To determine the effect of the errors in the CI+MBPT transition rates on the lifetime of the MOT, we randomly vary each of the 811 transition rates according to their expected error. Using these modified transition rates, we numerically solve the coupled differential equations to extract a MOT lifetime. We repeat this process 1000 times and report the mean and the standard deviation of the resulting MOT lifetimes.

### IV. EVALUATION OF THE STANDARD Ca MOT OPERATION

The standard implementation of a Ca MOT is formed by laser cooling on the strong  $4s4p \ ^1P_1 \leftarrow 4s^2 \ ^1S_0$  transition at 423 nm in the presence of an anti-Helmholtz magnetic field with gradient of 60 G/cm in the axial direction. This transition incurs loss from the laser cooling cycle primarily due to decay from the  $4s4p \ ^1P_1$  state to the  $3d4s \ ^1D_2$  state. This  $^1D_2$  state, as shown in Fig. 2, decays to the  $4s4p \ ^3P_1$  (83% branching) and  $^3P_2$  (17% branching) states with a total lifetime of 1.71 ms [19]. The  $^3P_1$  state decays to the ground state with a lifetime of 0.331 ms, while the  $^3P_2$  state has a lifetime of 118 minutes, leading to loss from the laser cooling cycle [19, 37]. This loss, which is proportional to the  $4s4p \ ^1P_1$  state population, limits the lifetime of the Ca MOT and according to the rate model with our experimental parameters leads to a MOT lifetime of 27(5) ms. As detailed later, we experimentally observe a MOT lifetime of 29(5) ms in this configuration.

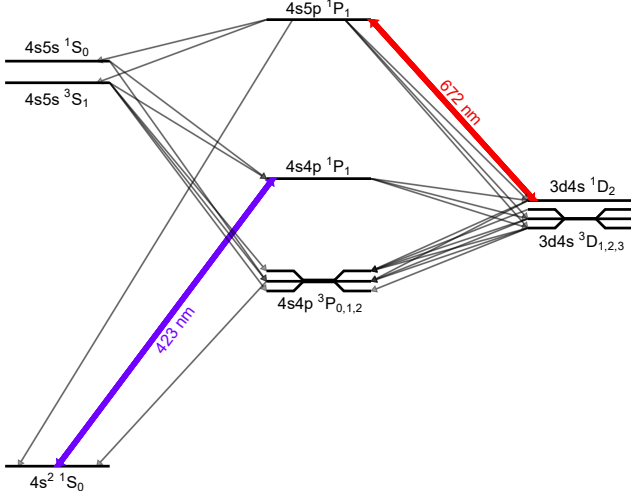


FIG. 2. Relevant level structure for operation of a standard calcium MOT. Laser cooling is accomplished on the 423 nm  $4s4p\ ^1P_1 \leftarrow 4s^2\ ^1S_0$  transition. Atoms that decay to the  $3d4s\ ^1D_2$  state are repumped back into the cooling cycle via the 672 nm  $4s5p\ ^1P_1 \leftarrow 3d4s\ ^1D_2$  transition, while those in the long-lived  $4s4p\ ^3P_{0,2}$  states are lost from the MOT.

To extend the MOT lifetime, a repumping laser is usually added to drive the  $4s5p\ ^1P_1 \leftarrow 3d4s\ ^1D_2$  transition at 672 nm in order to return electronic population in the  $3d4s\ ^1D_2$  level to the laser cooling cycle before it decays to the  $4s4p\ ^3P_1$  and  $^3P_2$  states [40]. In this configuration, the rate equation model predicts that the MOT lifetime is increased to 86(18) ms for our experimental parameters. As detailed later, we experimentally observe a MOT lifetime of 93(6) ms in this configuration.

Interestingly, it is often assumed that the lack of a further increase in the MOT lifetime with this repumping scheme is due to an incomplete depletion of the  $3d4s\ ^1D_2$  state, which is in turn due to unfavorable branching ratios in the  $4s5p\ ^1P_1$  state [40]; this state decays primarily back to the  $3d4s\ ^1D_2$  state and only weakly back in the cooling cycle. However, the rate equation model reveals that the MOT lifetime is actually limited by the decay of the  $4s5p\ ^1P_1$  state to the  $4s5s\ ^3S_1$ ,  $3d4s\ ^3D_1$ , and  $3d4s\ ^3D_2$  states, all of which decay primarily to the  $4s4p\ ^3P_{0,1,2}$  states, as shown in Fig. 2 and first pointed out in Ref. [41]. Specifically, according to the theoretical calculations, the  $4s5p\ ^1P_1$  state decays indirectly to the lossy  $4s4p\ ^3P_0$  and  $^3P_2$  states at a total rate of  $8 \times 10^4\ \text{s}^{-1}$ , while the  $3d4s\ ^1D_2$  state decays to the  $4s4p\ ^3P_2$  state at a rate of only  $80\ \text{s}^{-1}$ . With this understanding, the natural question arises: *Is there an alternative repumping scheme that would suppress the loss into these triplet states?*

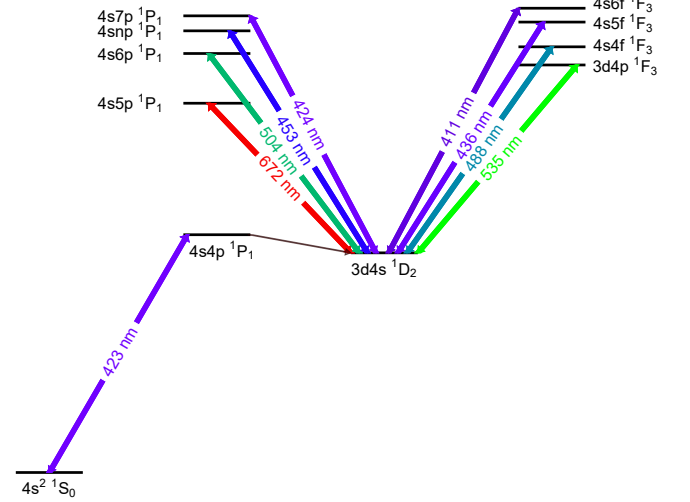


FIG. 3. Simplified calcium electronic level structure showing the eight repumping transitions considered here. All transitions except the 504 nm and 535 nm have been studied experimentally. The overall best Ca MOT performance is found when pumping to a highly configuration-mixed state, labeled as  $4snp\ ^1P_1$ , using the 453 nm  $4snp\ ^1P_1 \leftarrow 3d4s\ ^1D_2$  transition.

## V. EVALUATION OF ALTERNATIVE Ca MOT OPERATION SCHEMES

The ideal repumping laser out of the  $3d4s\ ^1D_2$  state would quickly transfer population from the  $^1D_2$  state back into the cooling cycle with perfect efficiency. With this idealized scheme, the rate model predicts a lifetime of 3.0(4) s with our MOT parameters. This lifetime is limited by the decay of the  $4s4p\ ^1P_1$  state to  $3d4s\ ^3D_1$  and  $^3D_2$  states and is thus dependent on the  $4s4p\ ^1P_1$  state population; lowering the  $4s4p\ ^1P_1$  state population by decreasing 423 nm cooling laser intensity while maintaining reasonable MOT performance can extend the lifetime by  $\sim 2\times$ . Since this lifetime is similar to lifetimes set by other effects in most systems, such as collisions with background gas, it is likely unnecessary for the majority of applications to employ a more complicated multi-laser repumping scheme out of the  $^3P$  states like that used in Sr [6], especially since the longer lifetime of the  $3d4s\ ^1D_2$  and  $4s4p\ ^3P_1$  in Ca make this scheme less efficient.

Therefore, for this work we choose to only explore single-laser repump transitions from the  $3d4s\ ^1D_2$  state with high branching ratios back into the laser cooling cycle. With this metric, we find that within the first 75 electronic states, there are seven reasonable alternative repumping transitions from the  $3d4s\ ^1D_2$  state, shown in Fig. 3, which go to states in the  $^1P_1$  and  $^1F_3$  manifolds. Using the rate equation model with our standard MOT parameters, we calculate the expected MOT lifetimes for these transitions, which are limited by optical pumping into the  $^3P_{0,2}$  states, and present the results in Table II.

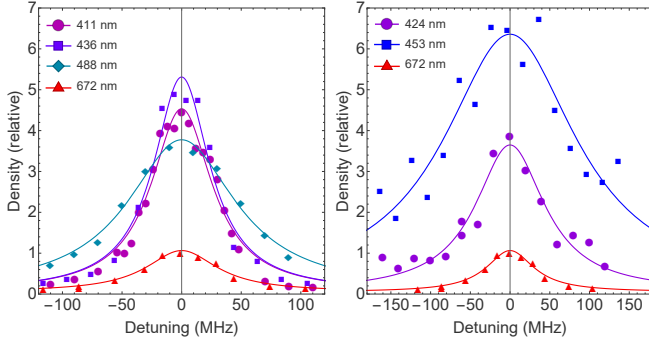


FIG. 4. Measured calcium MOT density as a function of repumping laser detuning for the (a)  $^1F_3$  and (b)  $^1P_1$  repump transitions. Experimental data are shown by points, while Lorentzian fits are shown as lines. All measured densities are scaled to the peak MOT density achievable with the standard 672 nm repumping scheme.

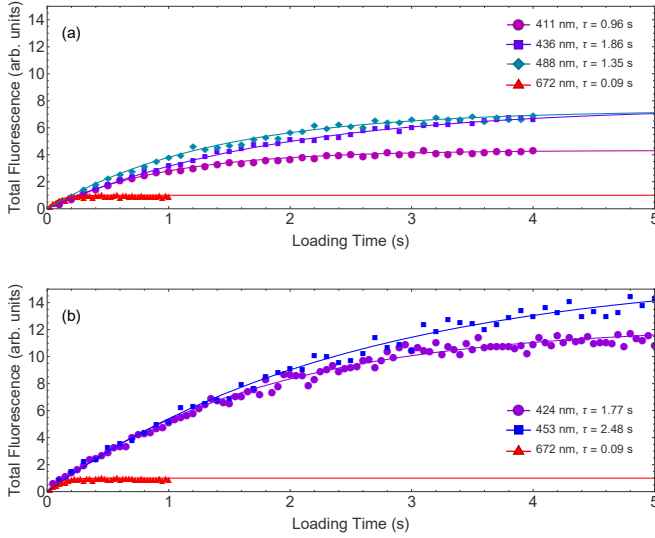


FIG. 5. Measured Ca MOT loading curves for the (a)  $^1F_3$  and (b)  $^1P_1$  repump transitions, MOT fluorescence is plotted as a function of time elapsed after the cooling lasers are turned on; curves fitted to  $N(t) = R\tau(1 - e^{-t/\tau})$  are shown alongside the data.

Of these seven transitions, five are accessible by lasers available to us and we explore them using a standard six beam Ca MOT described in Ref. [4]. Briefly, in this system, laser cooling is provided by driving the  $4s4p\ ^1P_1 \leftarrow 4s^2\ ^1S_0$  cooling transition with a total laser intensity of 63 mW/cm<sup>2</sup> detuned 34.4 MHz below resonance. The Ca MOT is loaded from an oven source placed  $\sim 3.5$  cm away from the MOT. Atoms from the oven are decelerated by two ‘deceleration beams’ with intensities 110 mW/cm<sup>2</sup> and 53 mW/cm<sup>2</sup> and detunings below resonance of 109 MHz and 318 MHz, respectively. The 672 nm traditional Ca MOT repump laser has an intensity of 11 mW/cm<sup>2</sup>.

For each single-beam repumping scheme, we characterize the MOT performance by measuring the MOT den-

sity, lifetime, and temperature. The density is measured using absorption imaging on the  $4s4p\ ^1P_1 \leftarrow 4s^2\ ^1S_0$  transition. The MOT lifetime,  $\tau$ , is extracted by using fluorescence imaging to observe the number of trapped atoms,  $N$ , as the MOT is loaded from the oven at rate  $R$  and fitting the data to the form  $N(t) = R\tau(1 - e^{-t/\tau})$ . The temperature,  $T$ , is found from the ballistic expansion of the Ca atoms after the MOT trapping beams are extinguished. For this measurement, the  $e^{-1}$  waist of the cloud is extracted from absorption images taken after a variable time of expansion, and  $T$  is extracted by fitting this data to the form  $w(t > 0) = \sqrt{w(t=0)^2 + \frac{2k_B T t^2}{m}}$ , where  $k_B$  and  $m$  are the Boltzmann constant and the mass of the Ca atom, respectively. The results of these measurements are shown in Fig. 4-5 and Table II. All of the experimentally explored alternative repumping schemes produce significantly denser MOTs at roughly the same temperature with longer lifetimes.

Somewhat surprisingly, repumping to  $^1F_3$  states leads to similar or sometimes better MOT performance than repumping to  $^1P_1$  states. Population promoted to the  $^1F_3$  states quickly decays to states with term  $^1D_2$ , which in turn primarily decay to the  $4s4p\ ^1P_1$  state. During this cascade, there is less decay into states of triplet character as compared to decays from some of the  $^1P_1$  repumping states. Thus, despite the more complicated repumping pathway, repumping to the  $^1F_3$  states can be very effective.

The relative performance of the  $^1F_3$  repumping schemes can be explained by their branching pathways into lossy triplet states. The total MOT loss rate due to loss from an upper repump state is given by  $\frac{d}{dt}N = -\Gamma_i f_{Loss} N_i$ , where  $N$  is the total number of atoms in the MOT,  $N_i$  is the number of atoms in the upper repump state,  $\Gamma_i$  is the natural linewidth of the upper repump state, and  $f_{Loss}$  is the fraction of decays which lead to decay into the triplet states directly or indirectly. Of the three  $^1F_3$  repump transitions experimentally tested, we approximate the relative values of  $N_i$  by comparing the average number of repump transition cycles required before decay into another state. We use the calculated linewidths  $\Gamma_i$  along with the most significant loss pathways to estimate  $f_{Loss}$ .

Summarizing from Fig. 6, the  $4s4f\ ^1F_3$  state decays with  $\sim 17\%$  branching into the  $4s4d\ ^1D_2$  state, which has a branching of  $\sim 0.2\%$  into the  $4s4p\ ^3P_2$  state. The  $4s5f\ ^1F_3$  state decays to the  $4s4d\ ^1D_2$ ,  $4p^2\ ^1D_2$ , and  $4s5d\ ^1D_2$  states with  $\sim 8\%$ ,  $\sim 3\%$ , and  $\sim 8\%$  branching, respectively. The  $4p^2\ ^1D_2$  state decays to triplet states with  $\sim 0.3\%$  branching, and the  $4s5d\ ^1D_2$  state decays to triplet states with  $\sim 0.1\%$  branching. The  $4s6f\ ^1F_3$  state decays with branching ratio  $\sim 5\%$ ,  $\sim 3\%$ ,  $\sim 5\%$ , and  $\sim 6\%$  into the  $4s4d\ ^1D_2$ ,  $4p^2\ ^1D_2$ ,  $4s5d\ ^1D_2$ , and  $4s6d\ ^1D_2$  states respectively, the last of which decays with  $\sim 0.6\%$  branching into the  $4s5p\ ^3P_1$  state. Using this method with only the branching ratios shown in Fig. 6 and the natural linewidths of the upper repump states, we predict that the lifetime of the MOT  $\tau_{488}$ ,  $\tau_{436}$ ,

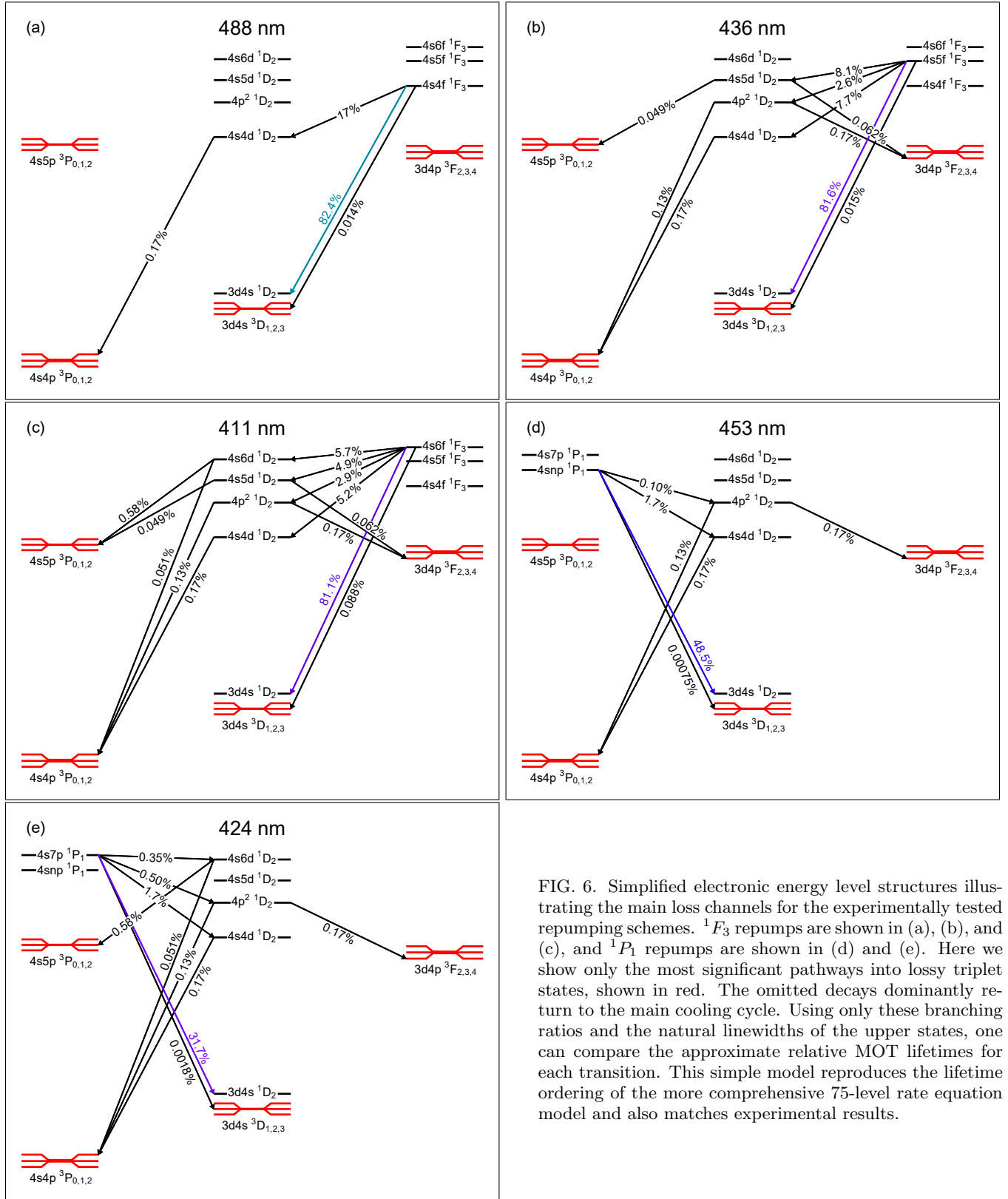


FIG. 6. Simplified electronic energy level structures illustrating the main loss channels for the experimentally tested repumping schemes.  $^1F_3$  repumps are shown in (a), (b), and (c), and  $^1P_1$  repumps are shown in (d) and (e). Here we show only the most significant pathways into lossy triplet states, shown in red. The omitted decays dominantly return to the main cooling cycle. Using only these branching ratios and the natural linewidths of the upper states, one can compare the approximate relative MOT lifetimes for each transition. This simple model reproduces the lifetime ordering of the more comprehensive 75-level rate equation model and also matches experimental results.



$\tau_{411}$ , using a 488 nm, 436 nm, or 411 nm repump should obey the relation:  $\tau_{436} > \tau_{488} > \tau_{411}$ . This agrees with the observed MOT lifetimes. For the same reason, we expect repumping to the  $3d4p\ ^1F_3$  state with a 535 nm laser will exhibit poor performance. One can use this method to quickly estimate relative performances of potential repump transitions without developing a comprehensive rate model.

Similarly, the MOT performance when repumping to the  $4s6p\ ^1P_1$  and  $4s7p\ ^1P_1$  states relative to the traditional  $4s5p\ ^1P_1$  state is understood by their primary branching ratios into triplet states. The  $4s6p\ ^1P_1$  state decays with  $\sim 0.006\%$  branching into the  $3d4s\ ^3D_2$  state, and the  $4s7p\ ^1P_1$  state decays with  $\sim 0.002\%$  branching into the  $3d4s\ ^3D_2$  state, while the  $4s5p\ ^1P_1$  state decays with  $\sim 0.9\%$  branching into the  $3d4s\ ^3D_1$ ,  $3d4s\ ^3D_2$ , and  $4s5s\ ^3S_1$  states.

Interestingly, the best MOT performance, in terms of number, density, and lifetime, is achieved by repumping to a highly configuration-mixed state, which we label as  $4snp\ ^1P_1$ . Our calculations find this state is primarily composed of the mixture  $4s7p$  (43%),  $4p3d$  (28%), and  $4s8p$  (13%). The high performance of this repumping transition arises from two facts. First, its primary branching ratio to triplet states is  $\sim 0.001\%$  and the lowest of all repumping transitions explored here. Second, it exhibits a very high branching ratio of  $\sim 43\%$  directly back to ground  $4s^2\ ^1S_0$  state.

Because the lifetime of the MOT when operating with the 453 nm repump ( $\sim 2.5$  s) is close to the idealized limit set by intercombination transitions from the  $4s4p\ ^1P_1$  state (3 s), we vary the intensity of the 423 nm cooling laser to measure the lifetime of the MOT as a function of the  $4s4p\ ^1P_1$  state population. Fig. 7 shows our results alongside the predicted lifetime from the rate model and the calculated limit of  $0.24/\rho_{pp}\text{ s}^{-1}$  set by the decay from the  $4s4p\ ^1P_1$  state indirectly to the lossy  $4s4p\ ^3P_0$  and  $^3P_2$  states – here  $\rho_{pp}$  is the population fraction in the  $4s4p\ ^1P_1$  state. Our results show that the lifetime of the MOT in this scheme approaches this fundamental limit for any Ca MOT with a single repump out of the  $3d4s\ ^1D_2$  state. Therefore, repumping at 453 nm provides nearly the optimum performance for any imaginable single-repump scheme in Ca.

Trapping calcium atoms in a MOT also provides us with a cold sample convenient for metastable state spectroscopy. We take advantage of this as well as the effect a repump laser has on the total number of atoms and fluorescence of a MOT to measure the transition energies of several repump transitions. Using a low repump laser intensity to minimize power broadening, we measure MOT fluorescence on the  $4s4p\ ^1P_1 \leftarrow 4s^2\ ^1S_0$  transition as we scan a given repump frequency. As the repump laser comes into resonance, the number of atoms in the MOT and the fluorescence drastically increase. We use a HighFinesse Angstrom WS Ultimate 2 wavelength meter calibrated to the Ca  $4s4p\ ^1P_1 \leftarrow 4s^2\ ^1S_0$  transition via a saturated absorption lock to measure the absolute fre-

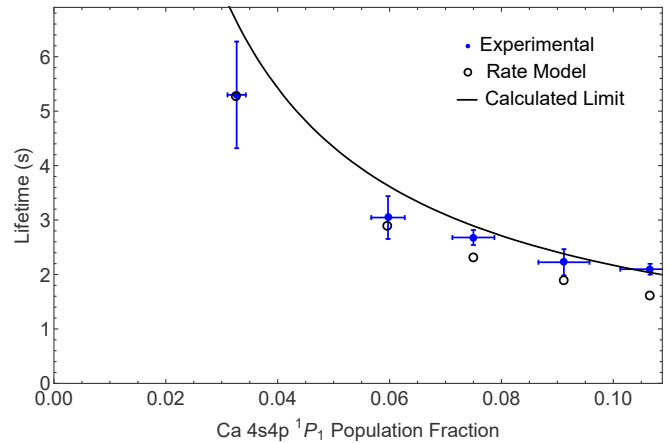


FIG. 7. Measured Ca MOT lifetime as a function of  $4s4p\ ^1P_1$  state population with a 453 nm repump. The measured lifetimes are shown alongside the rate model predictions and a curve representing the fundamental limit for any single repump laser scheme in a Ca MOT. This limit is the result of decay from the  $4s4p\ ^1P_1$  state indirectly to the  $4s4p\ ^3P_0$  and  $^3P_2$  states and is found as  $0.24/\rho_{pp}\text{ s}^{-1}$ , where  $\rho_{pp}$  is the population fraction of the Ca  $4s4p\ ^1P_1$  state.

quency [42]. Our results are shown in Table II, where the reported uncertainties account for the following potential errors: the absolute accuracy of the wavelength meter, the error in the Lorentzian fits, the Zeeman effect for a  $M_J = \pm 1$  transition, the DC Stark effect, the AC Stark effect, and the uncertainty in the Ca  $4s4p\ ^1P_1 \leftarrow 4s^2\ ^1S_0$  transition frequency.

## VI. Ca<sup>+</sup> PRODUCTION

Due to its relatively light mass and high ionization potential, Ca is especially useful in hybrid atom-ion traps as a sympathetic coolant [4]. However, as was recently identified [43, 44], Ca MOT operation can produce Ca<sup>+</sup> and Ca<sub>2</sub><sup>+</sup> through multi-photon and photo-associative ionization, respectively. These ions then produce an unwanted heat load during the sympathetic cooling process. While techniques exist to cope with these nuisance ions [44], it is advantageous to keep their production rate as low as possible. Therefore, we use time of flight mass spectrometry [45–47] to measure the density normalized Ca<sup>+</sup> production rate for each of the tested repump lasers and compare to the Ca<sup>+</sup> production rate with a 672 nm repump. As shown in Table II, we find that the largest Ca<sup>+</sup> production rate occurs with the 411 nm repump, a factor of 3.1 compared to the Ca<sup>+</sup> production rate with the 672 nm repump. The 453 nm repump, which resulted in the MOT with the longest lifetime, highest density, and largest number of atoms also yields the lowest Ca<sup>+</sup> production rate.



State	$\lambda$ (nm)	$f$ (THz)	$\rho_0$ (cm <sup>-3</sup> )	N	$\tau$ (s), model	$\tau$ (s), exp.	T (mK)	Ca <sup>+</sup> Production (relative)
$4s5p\ ^1P_1$	672	446.150837(13)	$7.5(7)\times 10^9$	$3.7(3)\times 10^6$	0.086(18)	0.093(6)	4(1)	$\equiv 1$
$3d4p\ ^1F_3$	535	—	—	—	0.14(11)	—	—	—
$4s6p\ ^1P_1$	504	—	—	—	2.3(3)	—	—	—
$4s4f\ ^1F_3$	488	614.393495(22)	$2.1(2)\times 10^{10}$	$2.7(2)\times 10^7$	0.73(16)	1.35(6)	5(1)	0.9(1)
$4snp\ ^1P_1$	<b>453</b>	<b>662.057231(22)</b>	<b><math>5.0(5)\times 10^{10}</math></b>	<b><math>7.8(7)\times 10^7</math></b>	<b>2.4(3)</b>	<b>2.48(8)</b>	<b>5(1)</b>	<b>0.8(1)</b>
$4s5f\ ^1F_3$	436	688.180929(22)	$2.8(3)\times 10^{10}$	$2.8(3)\times 10^7$	0.99(15)	1.86(7)	4(1)	1.4(2)
$4s7p\ ^1P_1$	424	706.783089(10)	$2.9(3)\times 10^{10}$	$5.9(5)\times 10^7$	2.2(3)	1.77(6)	5(1)	1.7(2)
$4s6f\ ^1F_3$	411	729.478413(22)	$2.5(2)\times 10^{10}$	$1.6(1)\times 10^7$	0.45(10)	0.96(3)	4(1)	3.1(4)
Ideal	—	—	—	—	3.0(4)	—	—	—

TABLE II. Summary of the results of this work. Each row of this table lists the calculated and measured properties of an individual repumping scheme, with the most efficient repump transition to the  $4snp\ ^1P_1$  state in bold. We attribute deviations between the model prediction for the MOT lifetime and the measured lifetime to inaccuracies in the calculated transition rates. These inaccuracies are expected to be higher for the high-lying  $F$ -states, in agreement with the larger deviations seen between model and data for these states. The experimental errors include statistical and systematic uncertainties.

## VII. SUMMARY

In summary, we propose seven alternatives to the traditional 672 nm repumping scheme for a Ca MOT and experimentally explore five of them. We find that all five produce significant improvements in MOT density and lifetime. Three of these repumping transitions appear particularly convenient from a technological perspective since they occur at wavelengths that are accessible by diode lasers, *i.e.* 453 nm, 424 nm, and 411 nm – with the middle transition of this list occurring at nearly the same wavelength as the cooling transition in Ca. The overall best MOT performance occurs for repumping at 453 nm on the  $4snp\ ^1P_1 \leftarrow 3d4s\ ^1D_2$  transition and results in a  $\sim 6\times$  and  $\sim 25\times$  improvement in density and lifetime, respectively, over the standard scheme. According to our rate model, this lifetime is near the maximum theoretical lifetime that can be achieved in a Ca MOT with a single repump laser from the  $3d4s\ ^1D_2$  state.

In all cases, the relative performance of the different repumping schemes can be understood by their branching into triplet states. Electronic population in these states typically ends up in either the  $4s4p\ ^3P_0$  or  $^3P_2$  state, which due to their long spontaneous emission lifetimes are lost from the MOT. For this reason, if a Ca MOT lifetime beyond that of  $\sim 5$  s is desired it would be necessary to add additional lasers to repump from the  $4s4p\ ^3P_0$  and  $4s4p\ ^3P_2$  states as is done in Sr [6]. If the MOT is not limited by other factors such as background gas collisions, we estimate this would extend the lifetime to  $\sim 29$  s. If a further increase in the lifetime is required, it would be necessary to repump from the  $4s4p\ ^3P_1$  state, which would completely close the laser

cooling cycle. However, even if these lasers are added, given the longer lifetime of the  $3d4s\ ^1D_2$  state as compared to its analogue in Sr, it will likely be necessary to retain the 453 nm repump for optimal MOT operation.

Finally, due to their similar atomic structure it may be possible to apply this repumping scheme in other Group 2(-like) atoms. For example, in Sr MOTs we speculate that repumping on the  $5s8p\ ^1P_1 \leftarrow 4d5s\ ^1D_2$  transition at 448 nm may be beneficial since it would return population from the  $4d5s\ ^1D_2$  more quickly than in the typically employed scheme and thereby increase the achievable optical force. A likely less efficient, but perhaps technologically simpler repumping pathway would be to drive the  $5s6p\ ^1P_1 \leftarrow 4d5s\ ^1D_2$  transition at 717 nm. In both of these cases, however, it may be necessary to retain the lasers used to repump population from the  $5s5p\ ^3P_0$  and  $^3P_2$  states as the larger spin-orbit mixing in Sr increases the parasitic intercombination transitions from *e.g.* the  $5s5p\ ^1P_1$  state.

## ACKNOWLEDGMENTS

We would like to thank M. Kozlov for help with the CI-MBPT package [38]. We also thank an anonymous referee for compiling a list of 111 experimentally measured transition rates for Ca I. This material is based upon work supported by the National Science Foundation Graduate Research Fellowship under Grant No. DGE-1650604. This work was supported by the National Science Foundation (PHY-1205311 and PHY-1607396) and Army Research Office (W911NF-15-1-0121 and W911NF-14-1-0378) grants. YMY thanks support of the National Natural Science Foundation of China, Grant No. 91536106.

[1] E. Raab et al., Phys. Rev. Lett. **59**, 2631 (1987).

[2] P. Hamilton et al., Science **349**, 849 (2015).

- [3] A. Kaufman et al., Science **353**, 794 (2016).
- [4] W. Rellergert et al., Nature **495**, 490 (2013).
- [5] J. Barry et al, Nature **512**, 286 (2014).
- [6] A. D. Ludlow, M. M. Boyd, J. Ye, E. Peik, and P. O. Schmidt, Rev. Mod. Phys. **87**, 637 (2015).
- [7] U. Sterr, C. Degenhardt, H. Stoehr, C. Lisdat, H. Schnatz, J. Helmcke, F. Riehle, G. Wilpers, C. Oates, and L. Hollberg, Comptes Rendus Physique **5**, 845 (2004).
- [8] C. Degenhardt, H. Stoehr, C. Lisdat, G. Wilpers, H. Schnatz, B. Lipphardt, T. Nazarova, P.-E. Pottie, U. Sterr, J. Helmcke, and F. Riehle, Phys. Rev. A **72**, 062111 (2005).
- [9] G. Wilpers, C. Oates, and L. Hollberg, Applied Physics B **85**, 31 (2006).
- [10] A. Vutha, New Journal of Physics **17**, 063030 (2015).
- [11] A. Derevianko and H. Katori, Rev. Mod. Phys. **83**, 331 (2011).
- [12] J. Grünert and A. Hemmerich, Applied Physics B **73**, 815 (2001).
- [13] G. Zinner, T. Binnewies, and F. Riehle, Phys. Rev. Lett. **85**, 2292 (2000).
- [14] G. Smith, J. Phys. B: At. Mol. Opt. Phys. **21**, 2827 (1988).
- [15] L. R. Hunter, G. M. Watson, D. S. Weiss, and A. G. Zajonc, Phys. Rev. A **31**, 2268 (1985).
- [16] G. Smith and D. S. J. Raggett, J. Phys. B: At. Mol. Phys. **14**, 4015 (1981).
- [17] W. H. Parkinson, E. M. Reeves, and F. S. Tomkinst, J. Phys. B: Atom. Molec. Phys. **9**, 157 (1976).
- [18] L. P. Lellouch and L. R. Hunter, Phys. Rev. A **36**, 3490 (1987).
- [19] D. Husain and G. Roberts, J. Chem. Soc., Faraday Trans. 2 **82**, 1921 (1986).
- [20] J. Mitroy, J. Phys. B: At. Mol. Opt. Phys. **26**, 3703 (1993).
- [21] T. Brage and C. F. Fischer, Phys. Rev. A **50**, 2937 (1994).
- [22] C. Laughlin and J. E. Hansen, J. Phys. B: At. Mol. Opt. Phys. **29**, L441 (1996).
- [23] J. E. Hansen, C. Laughlin, H. W. van der Hart, and G. Verbockhaven, J. Phys. B: At. Mol. Opt. Phys. **32**, 2099 (1999).
- [24] S. G. Porsev, M. G. Kozlov, Y. G. Rakhlina, and A. Derevianko, Phys. Rev. A **64**, 012508 (2001).
- [25] I. M. Savukov and W. R. Johnson, Phys. Rev. A **65**, 042503 (2002).
- [26] C. F. Fischer and G. Tachiev, Phys. Rev. A **68**, 012507 (2003).
- [27] H. Köstlin, Z. Phys. **178**, 200 (1964).
- [28] Aldenius, M., Lundberg, H., and Blackwell-Whitehead, R., Astron. Astrophys. **502**, 989 (2009).
- [29] L. R. Hunter and S. K. Peck, Phys. Rev. A **33**, 4452 (1986).
- [30] A. Kramida, Y. Ralchenko, J. Reader, and NIST ASD Team, “NIST Atomic Spectra Database (version 5.4),” (2016).
- [31] D. C. Morton, Astrophys. J. Suppl. Ser. **151**, 403 (2004).
- [32] G. Smith and J. A. O’Neill, Astron. Astrophys. **38**, 1 (1975).
- [33] K. Ueda, Y. Hamaguchi, and K. Fukuda, J. Phys. Soc. Jpn. **52**, 2666 (1983).
- [34] K. Ueda, Y. Hamaguchi, and K. Fukuda, J. Phys. Soc. Jpn. **51**, 2973 (1982).
- [35] V. A. Dzuba, V. V. Flambaum, and M. G. Kozlov, Phys. Rev. A **54**, 3948 (1996).
- [36] A. Derevianko and S. G. Porsev, in *Advances in Atomic, Molecular, and Optical Physics*, Vol. 60, edited by E. Arimondo, P. R. Berman, and C. C. Lin (Academic Press, 2011) pp. 415–459.
- [37] A. Derevianko, Phys. Rev. Lett. **87**, 023002 (2001).
- [38] M. G. Kozlov, S. G. Porsev, M. S. Safronova, and I. I. Tupitsyn, Comput. Phys. Commun. **195**, 199 (2015).
- [39] C. Foot, *Atomic physics*, Oxford master series in physics (Oxford University Press, 2005).
- [40] T. Kurosu and F. Shimizu, Jpn. J. Appl. Phys. **31**, 908 (1992).
- [41] C. Oates, F. Bondu, R. Fox, and L. Hollberg, The European Physical Journal D - Atomic, Molecular, Optical and Plasma Physics **7**, 449 (1999).
- [42] E. J. Salumbides, V. Maslinskas, I. M. Dildar, A. L. Wolf, E.-J. van Duijn, K. S. E. Eikema, and W. Ubachs, Phys. Rev. A **83**, 012502 (2011).
- [43] S. Sullivan et al, Phys. Chem. Chem. Phys. **13**, 18859 (2011).
- [44] S. Schowalter et al., Nature Comm. **7**, 124448 (2016).
- [45] S. Schowalter et al., Rev. Sci. Inst. **83**, 043103 (2012).
- [46] C. Schneider et al., Phys. Rev. App. **2**, 034103 (2014).
- [47] C. Schneider, S. J. Schowalter, P. Yu, and E. R. Hudson, International Journal of Mass Spectrometry **394**, 1 (2016).